THE JOURNAL OF PHYSICAL CHEMISTRY C

Article

Cite This: J. Phys. Chem. C 2019, 123, 12647−12658

pubs.acs.org/JPCC

Effect of an External Electric Field on the Fluorescence of a π-Conjugated Polymer Film of P3HT Sandwiched between FTO and PMMA

Published as part of The Journal of Physical Chemistry virtual special issue "Hai-Lung Dai Festschrift".

Kamlesh Awasthi,[†] Chin-Shiun Chiou,[†] Toshifumi Iimori,[‡] Eric Wei-Guang Diau,*[,†,§] and Nobuhiro Ohta*[,†,§]

[†]Department of Applied Chemistry and Institute of Molecular Science, National Chiao Tung University, 1001 Ta-Hsueh Road, Hsinchu 30010, Taiwan

[‡]Department of Applied Chemistry, Muroran Institute of Technology, Mizumoto-cho, Muroran 050-8585, Japan

[§]Center for Emergent Functional Matter Science, National Chiao Tung University, 1001 Ta-Hsueh Road, Hsinchu 30010, Taiwan

ABSTRACT: We report the photoexcitation dynamics of poly(hexylthiophene-2,5-diyl) (P3HT) as a solid film sandwiched between conducting films of a fluorine-doped tin-oxide-coated glass substrate (FTO) and an insulator film of poly(methyl methacrylate) (PMMA), from measurements of the effects of an external electric field on the absorption and photoluminescence (PL) spectra of P3HT. An Ag film was coated on the PMMA film; the FTO and Ag films served as electrodes to apply an external electric field to P3HT. According to the effects of a quadratic electric field, the lifetime of the emitting state of P3HT increased in the presence of that external field, resulting in an enhanced fluorescence quantum yield. An enhancement and quenching of fluorescence were observed also on applying an external electric field having the opposite polarity to the P3HT film between FTO and Ag films, which results from a field-induced change of both the population of the emitting state following photoexcitation and the rate of nonradiative decay at the emitting state. The dependence of the field-induced change of photoluminescence on the polarity of the applied external electric field between the FTO and Ag films was interpreted as an influence of an internal field located in the P3HT film sandwiched between FTO and PMMA films. These results of the effects of an electric field on the PL of a P3HT film sandwiched between FTO and PMMA films are compared with the effects on PL of P3HT sandwiched between a semiconductor film of TiO_2 or a Sb_2S_3 film and a PMMA film.

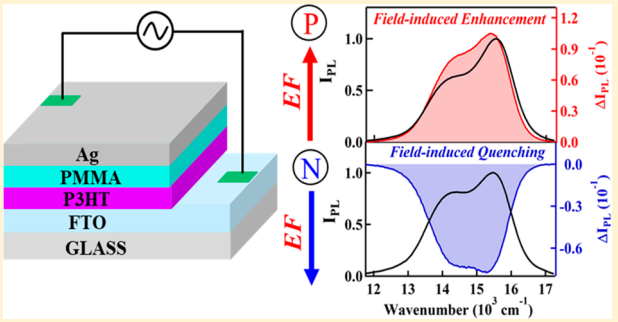

1. INTRODUCTION

π-Conjugated polymers, especially poly(hexylthiophene-2,5-diyl) (P3HT) and its derivatives, have received particular attention because they can serve as *p*-type organic semiconductors; they attract much interest for the development of a solid-state dye-sensitized solar cell (DSSC).[1−6] An understanding of the carrier dynamics and photochemical kinetics of these polymers following photoexcitation is important for the improvement of the performance of such a DSSC. To understand the photophysical and photochemical kinetics, electroabsorption (E-A) and electrophotoluminescence (E-PL) spectra, according to which a field induces a change of absorption and photoluminescence (PL), are useful; with these techniques, we reported a field-induced enhancement and quenching of fluorescence in a poly(phenylenevinylene) derivative depending on the excitation wavelength[7] and a field-induced modulation of the fluorescence of a P3HT film,[8] for which the enhancement and quenching of fluorescence were observed in the presence of the electric field in varied directions. In the latter work, E-PL spectra were recorded using both the first- and second-harmonic detections, i.e., on monitoring the field-induced changes that are proportional to the applied field strength linearly and quadratically, respectively; invaluable information was acquired about the importance of internal electric fields that are inherently present in the multilayer-film devices of DSSC.

We performed also time-resolved measurements of emission decay to investigate the linear (first-order) and quadratic (second-order) effects of an electric field on the decay profiles, to clarify the mechanism of the field-induced enhancement and quenching of emission. Our previous work[8] involved P3HT solid films sandwiched between a semiconductor layer of a mesoporous TiO_2 film or a TiO_2 film sensitized with Sb_2S_3 (namely, a Sb_2S_3 film) and an insulator film of poly(methyl

Received: March 29, 2019
Revised: April 27, 2019
Published: April 29, 2019

DOI: 10.1021/acs.jpcc.9b02946
J. Phys. Chem. C 2019, 123, 12647−12658

methacrylate) (PMMA). In those samples, the interfaces among P3HT, TiO_2, and Sb_2S_3 layers were present; TiO_2 and Sb_2S_3 films were deposited on a fluorine-doped tin oxide (FTO) coated glass substrate. In an investigation of the role of interfaces to TiO_2 and Sb_2S_3 in the generation of internal electric fields and in the photophysical and photochemical dynamics of P3HT, it is important to compare the results of the P3HT films sandwiched between semiconductor layers of TiO_2 or Sb_2S_3 and an insulator film of PMMA with the results of the P3HT films sandwiched between a conducting layer of FTO and an insulator film of PMMA.

In the present work, we studied the electronic structure and dynamics of a P3HT film sandwiched between FTO and PMMA films following photoexcitation with or without an applied electric field, based on the Stark spectra of P3HT in absorption and photoluminescence, that is, based on E-A and E-PL measurements. We compare the results with our previous results reported for a P3HT film sandwiched between TiO_2 or Sb_2S_3 and PMMA films. Figure 1 shows the layer structure of our present sample. We studied the second-order Stark effect on the absorption and PL spectra to study the quadratic electric-field effects including the Stark shift.[9,10] In addition, the first-harmonic detection was used to investigate the anisotropic internal fields that might exist in a thin-film device. We measured not only steady-state E-A and E-PL but also time-resolved E-PL, and examined the anisotropic behavior of the effect of an electric field on PL depending on the direction of the applied electric field.

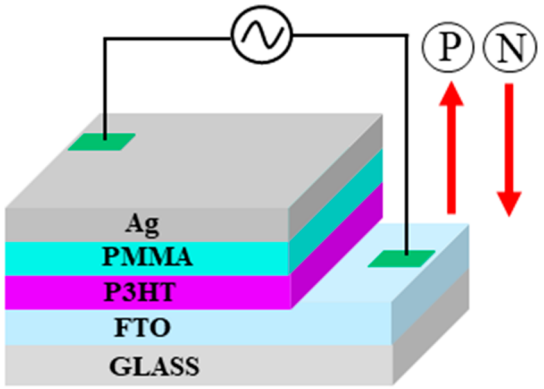

Figure 1. Layer structure of a device used for E-A and E-PL measurements. The positive and negative field directions mentioned in the text are shown with red arrows marked P and N, respectively.

2. EXPERIMENTS

2.1. Sample Preparation. The samples for the E-A and E-PL measurements were prepared as follows: (1) a part of the area of a FTO layer coated on a glass plate (Sinonar) was etched with zinc powder and HCl solution (4 M); (2) the plate was washed serially with detergent, a mixture of water, acetone, and 2-propanol, and deionized water, before cleaning with ultraviolet light and ozone; (3) a P3HT solid film was coated on the substrate with a spin-coating technique using P3HT solution, for which regioregular P3HT (15 mg, MW = 15000−45000, Rieke Metals) was dissolved in chlorobenzene (1 mL); (4) a PMMA film was deposited on the P3HT film using spin coating with PMMA solution (0.4 g in toluene, 10 mL); (5) a semitransparent Ag film of thickness ∼25 nm was deposited on the PMMA film using vacuum vapor deposition. PMMA (average MW = 120000, Aldrich) was purified on precipitation from a mixture of benzene and methanol and extraction with hot methanol. An external electric field was applied between the FTO and Ag films; FTO and Ag films served as electrodes. The thickness from the surface of FTO to the top layer of PMMA, which corresponds to the distance between the electrodes, was measured with a meter for surface roughness (Veeco Dektak 150).

2.2. Electroabsorption (E-A) and Electrophotoluminescence (E-PL) Spectra. All measurements were conducted near 23 °C. In absorption and E-A measurements, we used spectrometers (V570, JASCO and EMV-100, JASCO), as reported elsewhere.[11] On applying an electric field modulated with a function generator (Iwatsu, SG4311), a variation of the intensity of transmitted light for absorption was detected with a lock-in amplifier (Stanford Research, SR830).

E-PL spectra were recorded with PL spectra, with a fluorescence spectrometer (JASCO, FP777) combined with a lock-in amplifier, as reported elsewhere.[12] On applying a modulated electric field, a field-induced variation of the PL intensity was detected at the first and second harmonics of the modulation frequency, with a lock-in amplifier. The PL intensity at zero field and its field-induced change are hereafter represented by I_{PL} and ΔI_{PL} ($\equiv I_{PL}(F \neq 0) - I_{PL}(F = 0)$), respectively; here F is the strength of the applied electric field. E-PL spectra represent the plots of ΔI_{PL} as a function of wavelength (wavenumber).

2.3. PL Decay Profile with or without an Applied Electric Field. The time-resolved PL intensity in either the absence or presence of an applied electric field was measured with a single-photon-counting technique, as reported elsewhere.[13,14] The second harmonic of the femtosecond laser light from a mode-locked Ti:sapphire laser (Tsunami, Spectra Physics) pumped with a diode laser (Millennia Xs, Spectra Physics) served for excitation. The repetition rate of the laser pulse, which was originally 80 MHz, was decreased to ∼5.7 MHz with an electro-optic modulator (model 350-160, Conoptics). Emission from a sample following excitation with a laser pulse was dispersed with a monochromator (G-250, Nikon), and detected with a multichannel plate photomultiplier (R-3809U-52, Hamamatsu). A photon pulse originating from the emission served as an initial pulse in a time-to-amplitude converter (TAC, ORTEC); the monitored laser pulse served as a stopping pulse. Profiles of time-resolved decay were obtained on accumulating the output of the TAC with a multichannel analyzer (MCA7700, Seiko EG&G). To measure the effect of an electric field on the decay profile, we applied to a sample a voltage pulse train, which had a repetition of rectangular waves of positive, zero, negative, and zero bias. The memory channels of the MCA were divided into four segments; each segment stored a decay profile measured under a positive (CH1), zero (CH2), negative (CH3), or zero (CH4) bias, respectively. Hereafter, these decay profiles are represented as CH1, CH2, CH3, and CH4, respectively. To measure the decay profiles, we used a field strength $F = 0.3$ MV cm^{-1}. CH1 and CH3 then represent the decay profiles observed in the presence of +0.3 and −0.3 MV cm^{-1}, respectively, whereas CH2 and CH4 represent decay profiles observed at zero field. These positive and negative fields correspond to the positive and negative field directions, respectively (see Figure 1).

DOI: 10.1021/acs.jpcc.9b02946
J. Phys. Chem. C 2019, 123, 12647−12658

3. RESULTS

3.1. E-A Spectra. In a randomly oriented and immobilized system, a field-induced change in the absorption intensity of molecules and molecular aggregates is expressible according to the following equation, as a linear combination of the zeroth, first, and second derivatives of the absorption spectra.[9,15−17]

$$\Delta A(\nu) = (fF)^2\left[A_\chi A(\nu) + B_\chi \nu \frac{d(A(\nu)/\nu)}{d\nu} + C_\chi \nu \frac{d^2(A(\nu)/\nu)}{d^2\nu}\right] \quad (1)$$

Here, ν denotes the wavenumber of incident radiation, $A(\nu)$ absorbance at ν, f internal field factor, and F applied field strength. A_χ, B_χ, and C_χ are the coefficients of zeroth, first, and second derivatives of $A(\nu)$, respectively, which correspond to the variation of the absorption intensity, the spectral shift, and the spectral broadening. We performed the experiments at a magic-angle condition, $\chi = 54.7°$; χ is the angle between the applied electric field, $\boldsymbol{F}$, and the direction of polarization of the excitation light. P3HT in the solid film is assumed to be isotropically distributed and immobilized; the coefficients B_χ and C_χ reduce to

$$B_\chi \cong \frac{\Delta\bar{\alpha}}{2hc}, \quad C_\chi \cong \frac{|\Delta\boldsymbol{\mu}|^2}{6h^2c^2} \quad (2)$$

In these equations, $\Delta\bar{\alpha}$ is the trace of the difference of the molecular polarizability tensor between the excited and ground states; $\Delta\boldsymbol{\mu}$ is the difference of the electric dipole moments between the excited and ground states. With eq 2, $\Delta\bar{\alpha}$ and $|\Delta\boldsymbol{\mu}|$ are determined from the coefficients of the first and second derivatives, i.e., from B_χ and C_χ in the E-A spectra.

Figure 2 shows absorption and E-A spectra of the P3HT film sandwiched between FTO and PMMA films. The magnitude of ΔA is proportional to the square of the applied field strength, as shown in Figure 2d. An E-A spectrum simulated with eq 1 is shown in Figure 2c. The value of coefficient A_χ is as small as $\sim 2.0 \times 10^{-5}$ MV^{-2} cm^2, indicating that the transition moment of the absorption band is only slightly affected by $\boldsymbol{F}$, which is similar to the results of P3HT sandwiched between TiO_2 or Sb_2S_3 and PMMA films.[8] The values of $\Delta\bar{\alpha}$ and $|\Delta\boldsymbol{\mu}|$ for the electronic transition of P3HT were determined using eq 2, i.e., $f|\Delta\boldsymbol{\mu}| = 1.8$ D and $f^2\Delta\bar{\alpha} = 23$ Å^3. The magnitudes of the electric dipole moment and the polarizability in the excited state of P3HT are likely larger than those in the ground state. The significant magnitude of $f|\Delta\boldsymbol{\mu}|$ indicates an enhanced charge-transfer (CT) character following photoexcitation, but the present value of $f|\Delta\boldsymbol{\mu}|$ is smaller than the values obtained for P3HT films sandwiched between TiO_2 and PMMA films and between Sb_2S_3 and PMMA films, i.e., 2.6 and 2.9 D, respectively,[8] implying that the interfacial electron transfer from the excited state of P3HT to FTO is less efficient than that from the excited state of P3HT to a TiO_2 or Sb_2S_3 film. The simulated and observed E-A spectra deviate especially above 19 000 cm^{-1} (Figure 2c), which might arise from the difference in molecular parameters of $\Delta\bar{\alpha}$ and/or $|\Delta\boldsymbol{\mu}|$ between the aggregation and amorphous phases of P3HT.[18]

3.2. E-PL Spectra. Figure 3 shows an E-PL spectrum of P3HT sandwiched between FTO and PMMA observed at the second harmonic of the modulation frequency, together with the PL spectrum. The PL and E-PL spectra were simultaneously recorded with excitation at 450 nm with F =

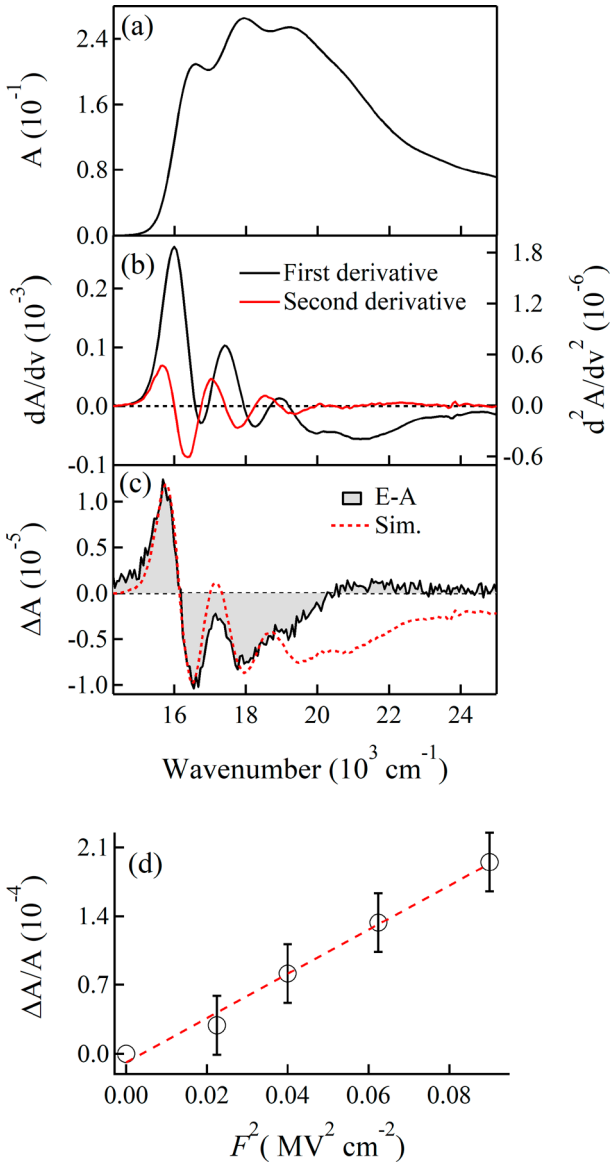

Figure 2. Absorption (a), first and second derivatives of the absorption spectrum (b), and E-A spectrum (c) of a P3HT solid film sandwiched between FTO and PMMA films; dependence on field strength at the E-A peak at 15800 cm^{-1} (d). The E-A spectrum shown in part c was recorded with an applied field strength of 0.3 MV cm^{-1}. In part c, the black solid line is the observed spectrum and the red broken line is the simulated spectrum.

0.3 MV cm^{-1}. The observed PL and E-PL spectra are reproduced well with two Gaussian profiles, i.e., with G1 and G2, as Figure 3 shows. E-PL spectra are typically reproduced with a linear combination of the zeroth, first, and second derivatives of the PL spectrum, as in the case of E-A spectra. As mentioned below, however, the shapes of observed E-PL and PL spectra are similar, indicating that the zeroth-derivative component is dominant. The PL intensity is hence significantly affected by an applied electric field. As the field-induced change in the PL intensity (ΔI_{PL}) relative to the unperturbed PL intensity (I_{PL}), i.e., $\Delta I_{PL}/I_{PL}$, gives the field-induced change in the emission quantum yield,[10] we can discuss how the photoexcitation dynamics are influenced by an applied electric field, based on the magnitude of $\Delta I_{PL}/I_{PL}$. The integrated intensities of the E-PL spectra are positive, indicating that the

DOI: 10.1021/acs.jpcc.9b02946
J. Phys. Chem. C 2019, 123, 12647−12658

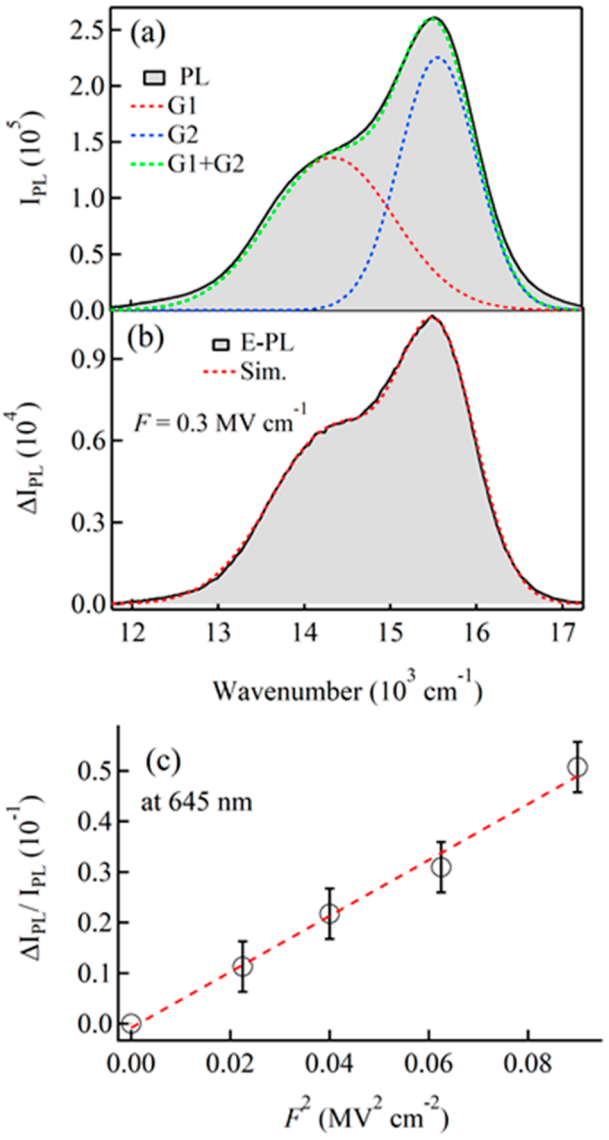

Figure 3. (a) PL spectrum of a P3HT solid film sandwiched between FTO and PMMA films, its decomposition to bands G1 (red dotted line) and G2 (blue dotted line) having Gaussian profiles, which were used for the simulation. (b) E-PL spectra (shaded line) at field strength 0.3 MV cm^{-1} and simulated spectra (red dotted line). (c) Plots of $\Delta I_{PL}/I_{PL}$ as a function of the squared strength of the applied field. G1 and G2 bands have maxima at 14049 and 15458 cm^{-1}, respectively.

PL quantum yield increases on application of an external electric field ($\boldsymbol{F}$), as a quadratic field effect. As shown in Figure 3c, the magnitude of $\Delta I_{PL}/I_{PL}$ is proportional to the square of the strength of the applied field.

The PL intensity ratio between G1 and G2 evaluated from the peak intensities of these bands, i.e., $I_{PL}(G1)/I_{PL}(G2)$, is about 0.60−0.75 (see Figure 3a); the magnitude of the field-induced change of the PL quantum yield, i.e., $\Delta I_{PL}/I_{PL}$, was estimated to be ∼0.052 and ∼0.053 at 0.3 MV cm^{-1} for G1 and G2, respectively, indicating that the PL quantum yield increases about 5% on application of field strength 0.3 MV cm^{-1}. ΔI_{PL} is given roughly by 0.58 $F^2 I_{PL}$ for both bands, as the quadratic field effect. Here F has units of MV cm^{-1}.

E-PL spectra were recorded also at the first harmonic of the modulation frequency; E-PL spectra were recorded for two directions of $\boldsymbol{F}$, for which the positive electrode was connected to FTO and negative electrode to silver, which is hereafter called as the positive field direction (indicated by P in Figure 1), and vice versa, called a negative field direction (indicated by N in Figure 1). The results given in Figure 4 clearly show that the effect of $\boldsymbol{F}$ on PL depends on the direction of $\boldsymbol{F}$. In the positive field direction, the intensity of the E-PL spectrum was positive (Figure 4b), indicating a field-induced increased quantum yield of PL for both G1 and G2. In the negative field direction, in contrast, the intensity of the E-PL spectrum was negative (Figure 4e), indicating a field-induced decreased quantum yield of PL for both G1 and G2, as a linear field effect. The magnitude of $\Delta I_{PL}/I_{PL}$ shows a linear dependence on field strength (see Figures 4c,f). The magnitude of $\Delta I_{PL}/I_{PL}$ caused by a linear field effect is roughly 0.1 with a field strength 0.3 MV cm^{-1} for both G1 and G2; ΔI_{PL} is hence roughly given as 0.33 FI_{PL} for both bands with unit MV cm^{-1} for F. To consider both linear and quadratic field effects, we express $\Delta I_{PL}/I_{PL}$ as

$$\Delta I_{PL}/I_{PL} = \pm 0.33F + 0.58F^2 \quad (3)$$

Here, the units of F are MV cm^{-1}; the plus and minus signs correspond to the directions of positive and negative applied field, respectively.

Although eq 3 is applicable for both G1 and G2, there is a small difference of magnitude of $\Delta I_{PL}/I_{PL}$ between G1 and G2; $\Delta I_{PL}/I_{PL}$ is a little larger for G1 than for G2 in both linear and quadratic field effects (see Figures 3 and 4). As shown below, the PL lifetimes monitored at these two bands differ from each other, indicating that emission arises from not a single electronic state, as in the case of P3HT sandwiched between TiO_2 and PMMA films and between Sb_2S_3 and PMMA films.[8] As shown in parts a and d of Figure 4, the relative intensities I_{PL} of G1 and G2 bands differ from each other. The relative intensity of the G1 band is comparable to that for the G2 band in Figure 4d but is smaller in Figure 4a. This difference is ascribed to experimental error due to the photobleaching of PL intensity; the efficiency of photobleaching differs somewhat between G1 and G2. PL and E-PL spectra shown in parts d and e of Figure 4, i.e., with a negative field direction, were recorded following the recording of PL and E-PL spectra shown in parts a and b of Figure 4, i.e., with a positive field direction. The ratio $\Delta I_{PL}/I_{PL}$ is unaffected by photobleaching, because PL and E-PL spectra were recorded concurrently.

As is discussed in the next section, PL decay measurements with or without an applied electric field show that the field-induced changes of both the population of the PL emitting state from the photoexcited state and the rate of nonradiative decay at the PL emitting state are the origin of the linear effects of the electric field on the PL intensity, i.e., on the PL quantum yield for both G1 and G2.

3.3. Field-Induced Change of the PL Decay Profile.

The field-induced variation of the PL decay profile of P3HT sandwiched between FTO and PMMA films was measured with field strength 0.3 MV cm^{-1} and excitation at 450 nm. The PL was monitored at 640 and 705 nm, which correspond to the intensity maxima of the G2 and G1 bands, respectively. Four decay profiles, i.e., CH1, CH2, CH3, and CH4, were obtained, as explained in Experiments. CH1 and CH3 represent the decay profiles observed in the presence of +0.3 and −0.3 MV cm^{-1}, respectively, whereas CH2 and CH4 represent the decay profiles observed at zero field. Hereafter, CH1 + CH3 and CH2 + CH4 are noted as $I(t)_{ON}$ and $I(t)_{OFF}$,

DOI: 10.1021/acs.jpcc.9b02946
J. Phys. Chem. C 2019, 123, 12647−12658

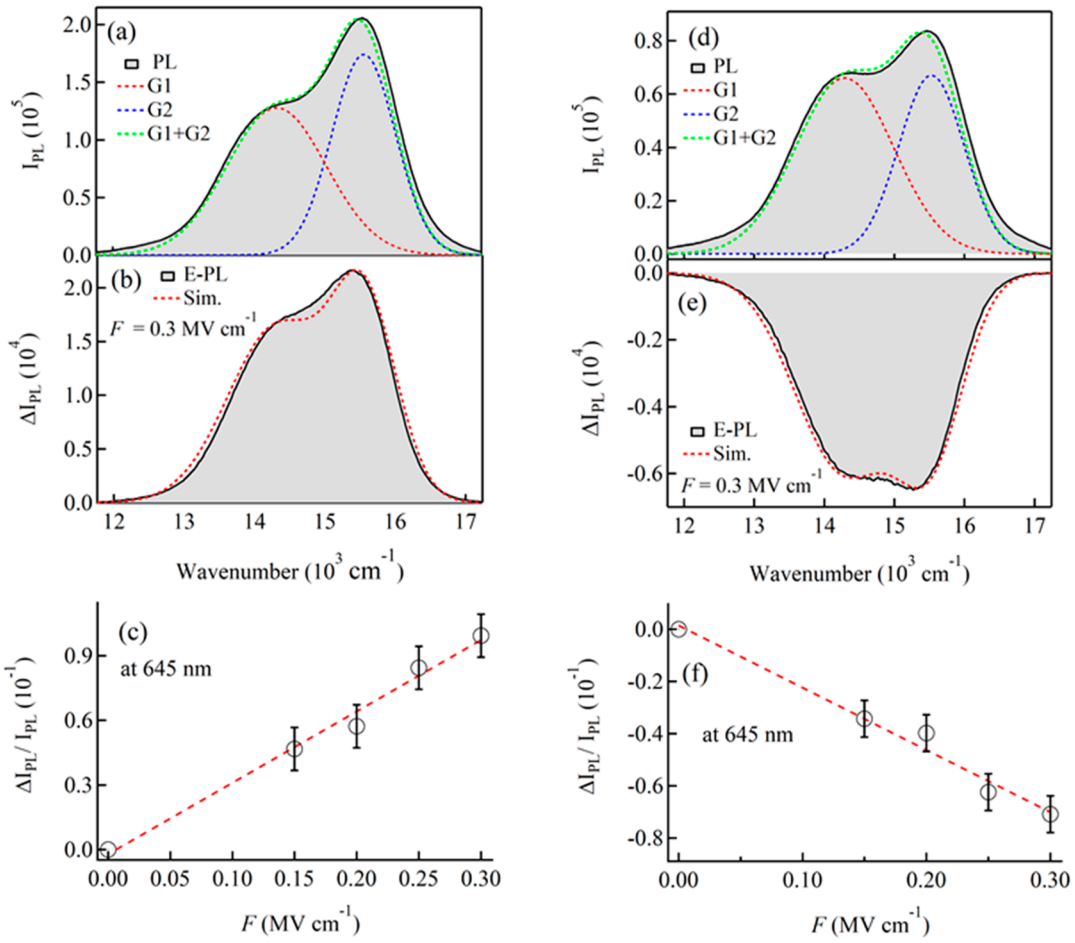

Figure 4. (a, d) PL spectra of a P3HT solid film sandwiched between FTO and PMMA films and its decomposition to bands G1 and G2 of Gaussian profiles. (b, e) E-PL spectra recorded with the first harmonic of the modulation frequency of an applied field of strength 0.3 MV cm^{-1} with positive field direction (b), negative field direction (e), and simulated E-PL spectra (red dotted line) as a sum of G1 and G2 bands. (c, f) Plots of $\Delta I_{PL}/I_{PL}$ as a function of applied electric-field strength. In these plots, the maximum intensity of G1 of the E-PL spectra was monitored. PL and E-PL spectra were concurrently recorded. The spectra observed with a field of negative direction were recorded following the recording with a field of positive direction.

respectively. Figure 5 shows the decay profiles of $I(t)_{ON}$, $I(t)_{OFF}$, $I(t)_{ON} - I(t)_{OFF}$, and $I(t)_{ON}/I(t)_{OFF}$. $I(t)_{OFF}$ presents the decay profile at zero field. As the linear field effect that shows the opposite dependence on field direction is canceled on adding CH1 and CH3, $I(t)_{ON}$ gives the decay that includes only the quadratic field effect.

The decay profiles of $I(t)_{ON}$ and $I(t)_{OFF}$ were simulated on assuming a triexponential decay, that is, $\sum_{i=1}^{3} A_i \exp(-t/\tau_i)$, in which t denotes time, τ_i lifetime, and A_i the pre-exponential factor of component i. The average lifetimes (τ_{ave}) given by $\tau_{ave} = \sum_{i=1}^{3} A_i\tau_i / \sum_{i=1}^{3} A_i$ were derived also from $I(t)_{ON}$ and $I(t)_{OFF}$. These results are shown in Table 1. We determined parameters τ_i and A_i on simulating the profiles of not only $I(t)_{ON}$ and $I(t)_{OFF}$ but also their difference and ratio, i.e., $(I(t)_{ON}\text{-}I(t)_{OFF})$ and $(I(t)_{ON}/I(t)_{OFF})$. $I(t)_{ON} - I(t)_{OFF}$ is regarded as the time-resolved E-PL signal taken at the second harmonic of the modulation frequency, which corresponds to the E-PL spectrum shown in Figure 3b.

As shown in Figures 5 c, g, $I(t)_{ON} - I(t)_{OFF}$ is positive in the entire time region for both G1 and G2, indicating the field-induced enhanced emission components that give G1 and G2, in agreement with the steady-state E-PL spectra recorded at the second harmonic of the modulation frequency of $\boldsymbol{F}$ (see Figure 3b). As shown in Table 1, the summation of A_i, i.e., $\sum_{i=1}^{3} A_i$, at 0.3 MV cm^{-1} is nearly the same as that at zero field at both G1 and G2, indicating that the population of the emitting state of both emissions is little affected by $\boldsymbol{F}$, in the quadratic field effect.

This effect is clearly perceptible in the decay profiles, as the magnitude of $I(t)_{ON}/I(t)_{OFF}$ is nearly unity at $t = 0$ for both G1 and G2 (see Figure 5d,h). Unlike the population of the emitting state, the PL lifetime is affected by $\boldsymbol{F}$; that is, the average lifetime increases in the presence of $\boldsymbol{F}$ for both G1 and G2 (see Table 1). In the results, $I(t)_{ON}/I(t)_{OFF}$ increases with increasing time, t. PL intensity is hence enhanced with an applied electric field for both G1 and G2, as the quadratic field effect, which originates from the field-induced deceleration of the nonradiative process at the emitting states of G1 and G2. Regarding the quadratic field effect on PL, the P3HT film sandwiched between FTO and PMMA films shows a behavior similar to that of a P3HT film sandwiched between TiO_2 and PMMA films or between Sb_2S_3 and PMMA films. The magnitude of ΔI_{PL} relative to I_{PL} estimated from the decay in interval 0−1 ns, shown in Figure 5, is about 3% with field strength 0.3 MV cm^{-1} for both G1 and G2. This value is near that estimated from the steady-state PL and E-PL spectra

DOI: 10.1021/acs.jpcc.9b02946
J. Phys. Chem. C 2019, 123, 12647−12658

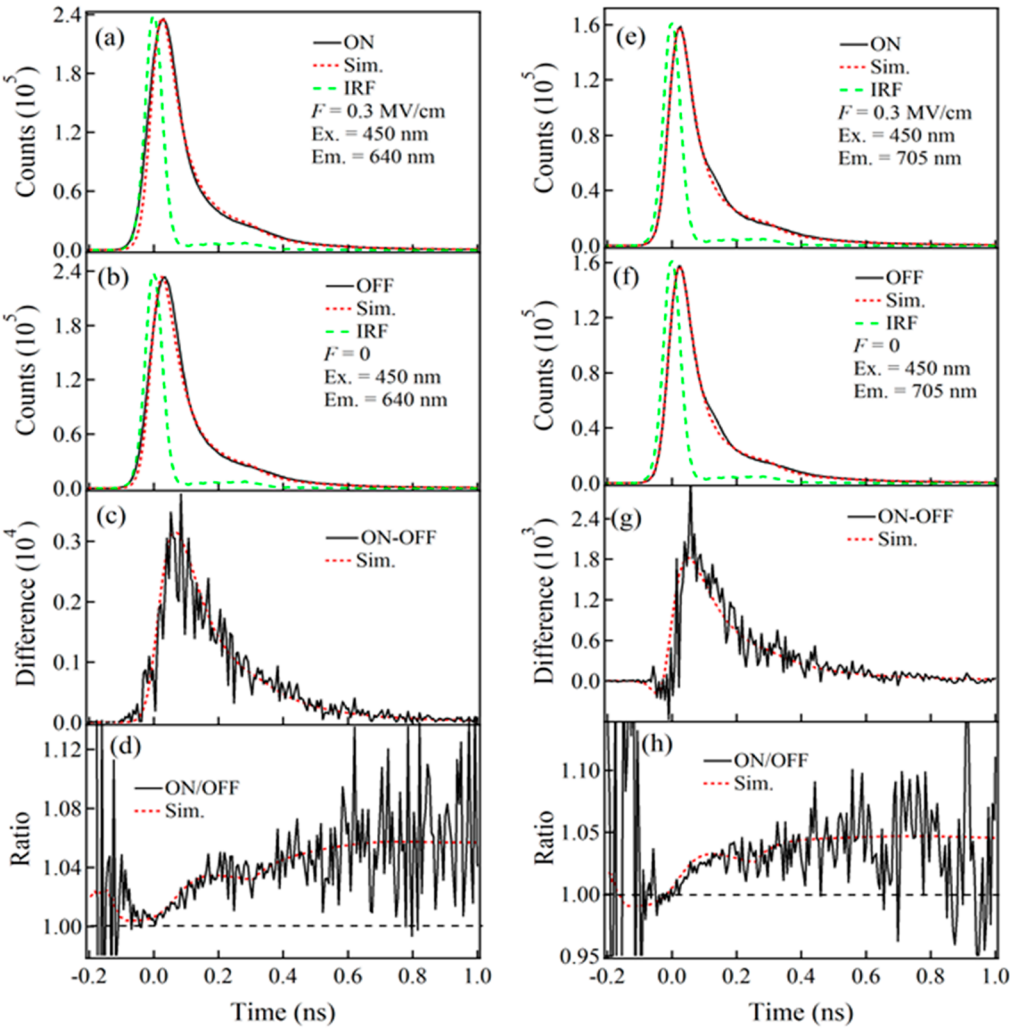

Figure 5. PL decay profiles of a P3HT sold film sandwiched between FTO and PMMA films. (a, e) Decay profile observed in the presence of field 0.3 MV cm^{-1} (black solid line), simulated curve (red dotted line), and instrument response function (green broken line), (b, f) decay profiles observed at zero field (black solid line), simulated curve (red dotted line), and instrument response function (green broken line), (c, g) difference between the two decay profiles at zero field and at 0.3 MV cm^{-1}, i.e., $I(t)_{ON} - I(t)_{OFF}$ (black solid line) and simulated curve (red dotted line), and (d, h) ratio between the two decay profiles, i.e., $I(t)_{ON}/I(t)_{OFF}$ (black solid line) and a simulated curve (red dotted line). The results in the left and right columns were obtained on monitoring PL at 640 and 705 nm, respectively. The decay at zero field was obtained from CH2 + CH4, whereas the decay at 0.3 MV cm^{-1} was obtained from CH1 + CH3. See the text for details.

Table 1. Lifetime τ_i and Pre-Exponential Factor (in Parentheses) of Each Decay Component of PL Observed at Field Strength 0.3 MV cm^{-1} Measured as $I(t)_{ON}$ = CH1 + CH3, and at Zero Field Measured as $I(t)_{OFF}$ = CH2 + CH4[a)]

λ/nm	F/MV cm^{-1}	τ_1/ps (A_1)	τ_2/ps (A_2)	τ_3/ps (A_3)	τ_{ave}/ps
640	0.3	51.4 (0.790)	146.5 (0.206)	565.3 (0.005)	73.6 ± 2.0
	0	50.3 (0.790)	143.8 (0.205)	541.9 (0.005)	72.0 ± 1.8
705	0.3	41.2 (0.792)	128.0 (0.193)	409.5 (0.016)	63.7 ± 2.4
	0	40.8 (0.798)	127.1 (0.186)	401.4 (0.016)	62.6 ± 2.0

[a)]The average lifetime (τ_{ave}) in each decay profile is also shown. The sums of the pre-exponential factors are normalized to unity for the decay profile at zero field. The PL was monitored at wavelengths λ = 640 and 705 nm, respectively, for bands G1 and G2. The experimental error of lifetime and pre-exponential factor of each decay component is estimated to be ±5%.

shown in Figure 3, indicating that rapidly decaying components are efficiently affected by an applied electric field.

Figure 4 shows that E-PL spectra observed at the first harmonic of the modulation frequency of the applied AC voltage exhibit a marked difference between the E-PL spectra recorded for the opposite field directions. Each decay profile of CH1 and CH3 involves both the linear and quadratic effects of the field, whereas CH1 + CH3 shows only a quadratic field effect because the linear field effect is canceled. CH1 − (CH1 + CH3)/2 and CH3 − (CH1 + CH3)/2, which result in (CH1 − CH3)/2) and (CH3 − CH1)/2), respectively, hence involve only a linear field effect, because the quadratic field effect is removed. These decay profiles and their ratio relative to the decay at zero field, i.e., [(CH1 − CH3)]/[(CH2 + CH4)] and [(CH3 − CH1)]/[(CH2 + CH4)], are shown in Figure 6. The ratio is not unity at t = 0 and gradually increases

DOI: 10.1021/acs.jpcc.9b02946
J. Phys. Chem. C 2019, 123, 12647−12658

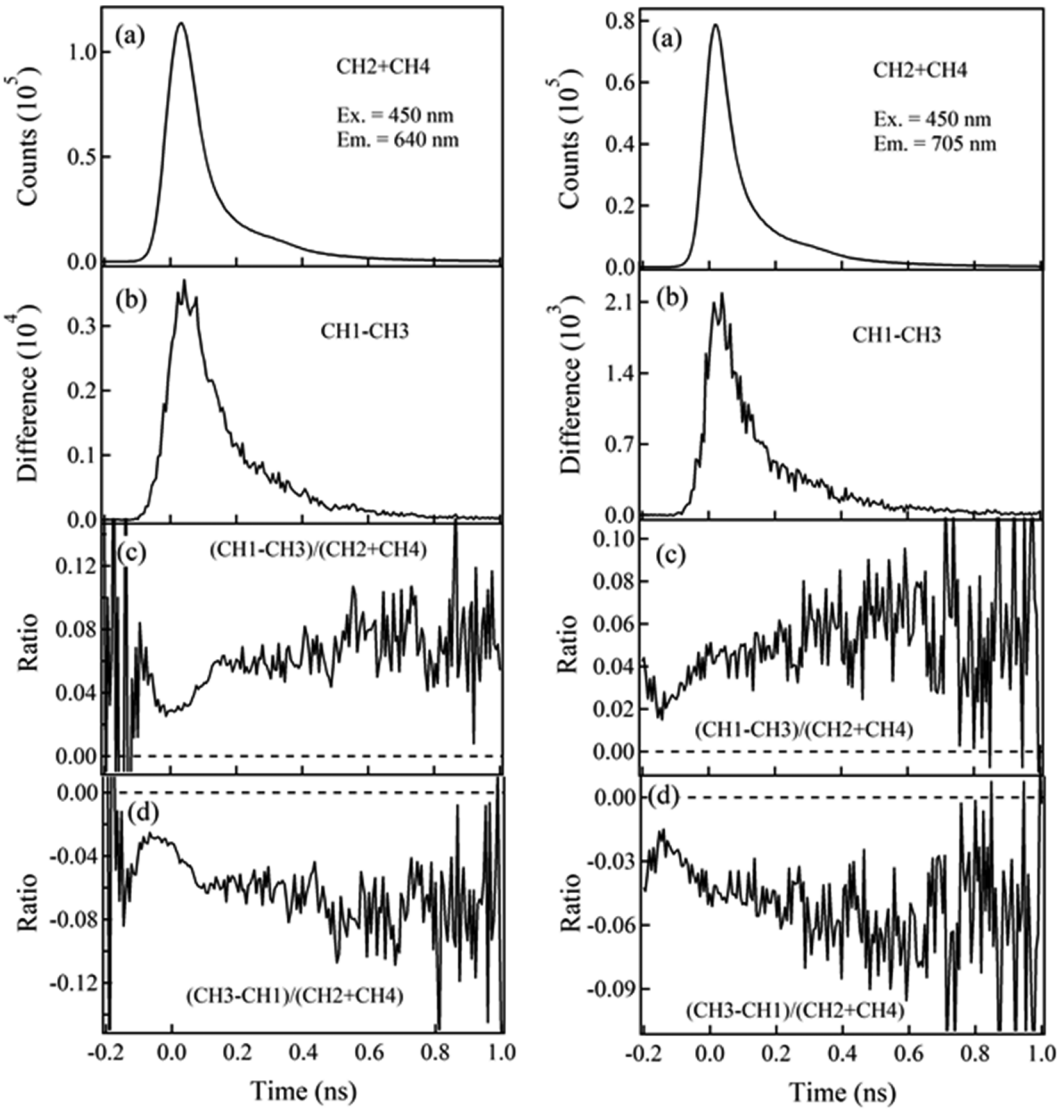

Figure 6. PL decay profiles of a P3HT solid film sandwiched between FTO and PMMA films monitored at 640 (left) and 705 (right) nm, and their field effect. (a) Decay profile observed at zero field, (b) difference between the decay profiles observed with positive and negative field directions, i.e., (CH1 − CH3), (c) ratio of (CH1 − CH3) relative to the decay at zero field, i.e., (CH1 − CH3)/(CH2 + CH4), and (d) ratio of (CH3 − CH1) relative to the decay at zero field, i.e., (CH3 − CH1)/(CH2 + CH4). The decay profile at zero field was obtained from [CH2 + CH4]/2, whereas the decay profiles at +0.3 and −0.3 MV cm^{-1} were obtained from CH1 and CH3, respectively. See the text for details.

or decreases, respectively, as a function of time, indicating that both the population of the emitting state and the lifetime of PL are affected by ***F*** for both G1 and G2. The fact that the decay of CH1− CH3 or CH3 − CH1 shows positive or negative values in the entire time region indicates that PL is enhanced or quenched by ***F*** having a positive or negative direction, respectively, as the linear field effect. These results are consistent with the E-PL spectra recorded at the first harmonic of the modulation frequency of ***F*** in a positive or negative direction (see Figure 4).

The decay profiles of [(CH2 + CH4) + (CH1 − CH3)] and [(CH2 + CH4) + (CH3 − CH1)] were simulated on assuming a triexponential decay (see Figure 7). [(CH2 + CH4) + (CH1 − CH3)] and [(CH2 + CH4) + (CH3 − CH1)] correspond to the PL decay influenced by the linear field effect, because (CH2 + CH4) corresponds to the decay at zero field and (CH1 − CH3) represents the field-induced change caused by the linear field effect. The results appear in Table 2. The sum of the pre-exponential factors, i.e., $\sum_{i=1}^{3} A_i$, at +0.3 MV cm^{-1} is a little larger than that at zero field for both G1 and G2 (see Table 2); in contrast, this value is a little smaller at −0.3 MV cm^{-1} than that at zero field for both G1 and G2. These results show that the sum of the pre-exponential factors of decaying components increases or decreases for both G1 and G2, respectively, on application of an external field having positive or negative field directions. The population of the PL emitting states of G1 and G2 following photoexcitation hence increases or decreases, respectively, when an external electric field is applied in a positive or negative direction. This effect is confirmed also in Figure 6c, because (CH1 − CH3)/(CH2 + CH4) is not zero at t = 0. The population of the PL emitting states of G1 and G2 is clearly affected with an external field, as a linear field effect. Furthermore, the PL lifetime increases or decreases, respectively, on application of an external field in the positive or negative direction for both G1 and G2, as a linear field

DOI: 10.1021/acs.jpcc.9b02946
J. Phys. Chem. C 2019, 123, 12647−12658

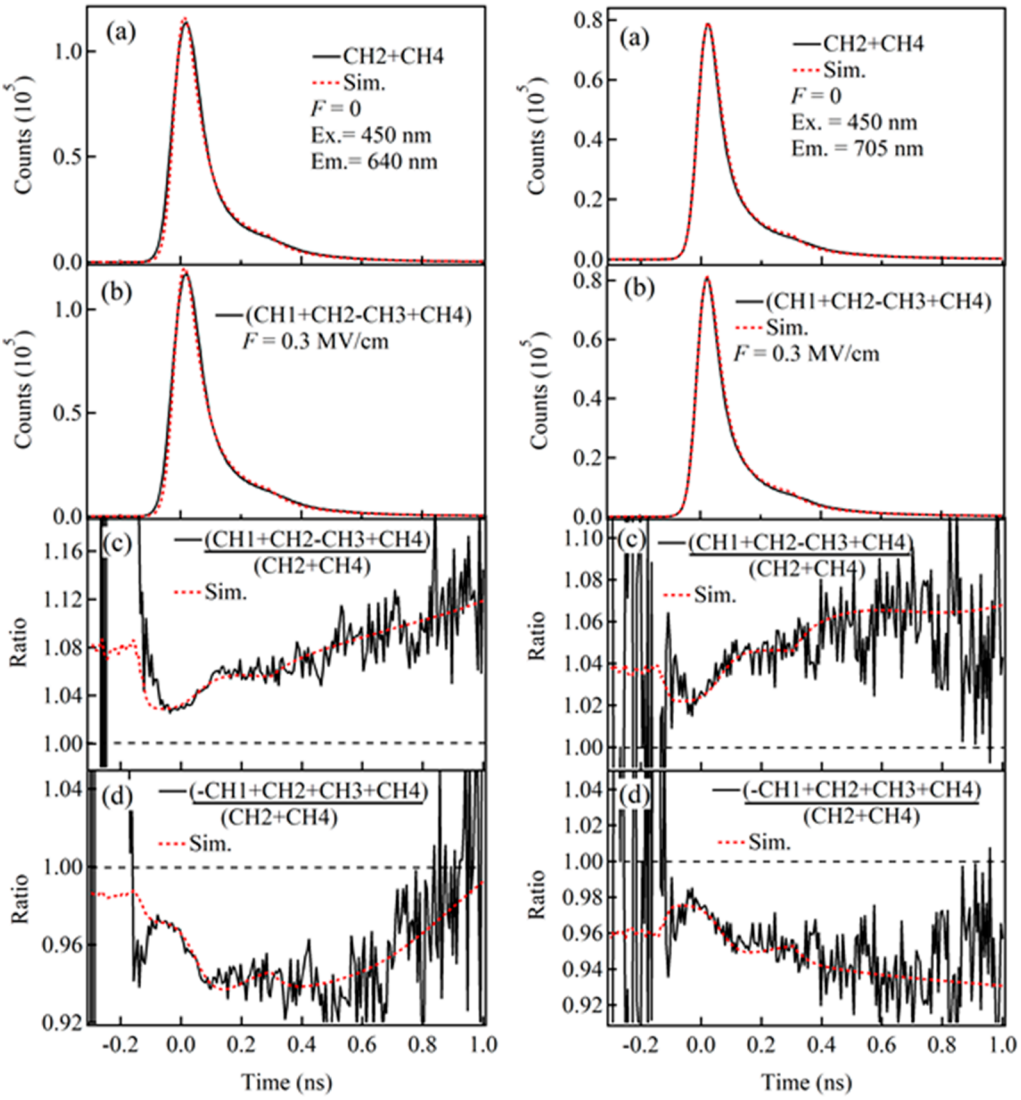

Figure 7. PL decay profiles of a P3HT solid film sandwiched between FTO and PMMA films. Their field effect corresponds to a linear field effect. The PL was monitored at 640 and 705 nm, respectively, in the left and right columns. (a) Decay profile at zero field, (b) decay profiles that include a linear field effect at 0.3 MV cm^{-1}, i.e., [(CH2 + CH4) + (CH1 − CH3)], (c) ratio of [(CH2 + CH4) + (CH1 − CH3)] relative to (CH2 + CH4), and (d) ratio of [(CH2 + CH4) − (CH1 − CH3)] relative to (CH2 + CH4). (CH2 + CH4) corresponds to the decay at zero field and CH1 and CH3 show the decay profiles at +0.3 and −0.3 MV cm^{-1}, respectively. See the text for details.

Table 2. Lifetime τ_i and Pre-Exponential Factor (in Parentheses) of Each Decay Component of PL Observed at Field Strength 0.3 MV cm^{-1}[a]

λ/nm	F /MV cm^{-1}	τ_1/ps (A_1)	τ_2/ps (A_2)	τ_3/ps (A_3)	τ_{ave}/ps ($\sum_{i=1}^{3}A_i$)
640	+0.3	51.2 (0.810)	146.6 (0.211)	580.2 (0.005)	73.4 (1.026)
	0	50.3 (0.790)	143.8 (0.205)	541.9 (0.005)	71.9 (1.000)
	−0.3	48.7 (0.770)	141.5 (0.200)	545.5 (0.005)	70.3 (0.975)
705	+0.3	41.5 (0.815)	130.7 (0.189)	414.4 (0.016)	63.9 (1.020)
	0	40.8 (0.798)	127.1 (0.186)	401.4 (0.016)	62.6 (1.000)
	−0.3	40.2 (0.785)	126.5 (0.178)	398.2 (0.015)	61.4 (0.978)

[a]The simulation was made for the decay of [(CH2 + CH4) + (CH1 − CH3)] for a positive field direction and for the decay of [(CH2 + CH4) − (CH1 − CH3)] for a negative field direction. The average lifetime (τ_{ave}) and the sum of the pre-exponential factors ($\sum_{i=1}^{3}A_i$) in each decay profile are also shown. The sum of the pre-exponential factors is normalized to unity for the decay profile at zero field. The PL was monitored at wavelengths λ = 640 and 705 nm for bands G1 and G2, respectively. Experimental error is estimated to be ±5% for both lifetime and pre-exponential factor.

effect. We hence recognize the anisotropic behavior of the field-induced change in PL decay parameters of P3HT sandwiched between FTO and PMMA films, which depends on the direction of an applied field.

4. DISCUSSION

Both ordered crystalline aggregates and amorphous P3HT chains have been suggested, experimentally and theoretically,

DOI: 10.1021/acs.jpcc.9b02946
J. Phys. Chem. C 2019, 123, 12647−12658

to coexist in the film.[19] In the absorption spectra of our samples, the vibronic bands appearing below 19 000 cm^{-1} are ascribed mainly to crystalline aggregates of P3HT (Figure 2) whereas a broad absorption for the amorphous state overlaps above 20 000 cm^{-1}.

The photoexcitation dynamics and effects of an electric field on the PL of a P3HT solid film sandwiched between FTO and PMMM are explicable using the reaction scheme shown in Figure 8. P3HT in the amorphous state might be excited

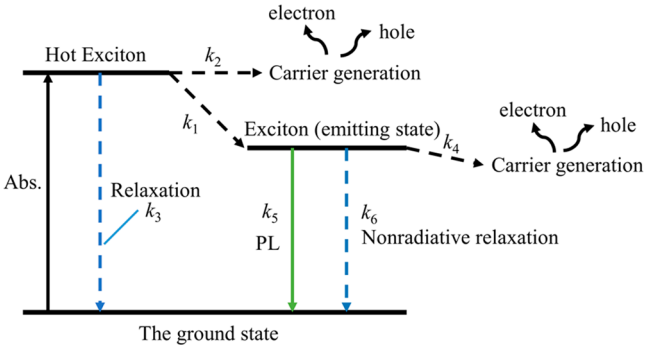

Figure 8. Schematic representation of the relaxation paths of P3HT upon excitation.

mainly at wavelength 450 nm. The energy transfer from the amorphous state to the crystalline aggregates is assumed to be so rapid and efficient that the PL decay reflects the kinetics in only the crystalline aggregates of P3HT. Here, excitons of two kinds are considered, that is, a hot exciton and a relaxed exciton.[20] The former is the bound electron−hole pair produced just following photoexcitation; the latter is the exciton produced on relaxation from a hot exciton. The observed PL of a P3HT solid film is emitted from the latter exciton. The former exciton is considered to dissociate (carrier generation), in competition with the relaxation to the relaxed exciton and the relaxation to the ground state. Carrier generation might occur also from the latter exciton, in competition with the radiative and nonradiative processes to the ground state, as shown in Figure 8.

According to the quadratic field effect, the PL intensity (quantum yield) and the PL lifetime increase in the presence of an applied electric field. This effect is explicable on considering that the nonradiative process at the emitting state (exciton) decreases with an applied electric field. An exciton is regarded as a kind of electron−hole pair; the nonradiative transition of an exciton to relax to the ground state might resemble a back-electron transfer. This process might be diminished on application of an electric field. Our extensive investigation of the effects of an electric field on the photoinduced electron transfer and back-electron transfer shows that these processes are affected with an electric field[21,22] as a quadratic field effect. The effects of the electric field on the rate of electron-transfer reactions originate from the change in the difference of Gibbs energies, that is, ΔG between neutral and charge-separated states on application of an electric field. Because charge-separated states have a larger dipole moment than neutral states, the Stark shift for the charge-separated state increases, which alters ΔG in the presence of an electric field. The rate of the back electron-transfer reaction would decrease upon a field-induced change of ΔG, which is similar to the so-called inverted region in the theory of electron transfer. As the initial population of the PL emitting state showed no quadratic field effect, the relaxation of a hot exciton to the exciton-emitting state and carrier generation from a hot exciton, of which the rate coefficients are given as k_1 and k_2 in Figure 8, respectively, show no quadratic field effect.

The PL of P3HT sandwiched between FTO and PMMA films shows a linear field effect, as in the case of the PL of P3HT sandwiched between TiO_2 and PMMA films or between Sb_2S_3 and PMMA films; the PL intensity and lifetime vary in the presence of $\boldsymbol{F}$, depending on the direction of an applied field. When the electric field was applied along the positive direction, the PL intensity increased, which resulted from both the field-induced increase of the population of the emitting state and the field-induced increase of the lifetime. When an electric field was applied along the negative direction, in contrast, the population of the emitting state and the PL lifetime decreased, resulting in a field-induced quenching of the PL. In Figure 8, the field-induced increase or decrease of the population of the PL emitting state indicates the field-induced increase or decrease of the magnitude of $k_1/(k_1 + k_2 + k_3)$, respectively, which likely arises from the field effect on carrier generation, i.e., on k_2. This process corresponds to one relaxation path of the hot exciton. The field-induced increase or decrease of the PL lifetime indicates the field-induced increase or decrease of the magnitude of $1/(k_4 + k_5 + k_6)$, respectively, which likely arises from the field effect on carrier generation, i.e., on k_4. On applying an electric field, the dissociation of the exciton generally becomes enhanced in π-conjugated polymers;[23,24] k_2 and k_4 in Figure 8 likely increase in the presence of an electric field. The relaxation path of the hot exciton is affected by the electric fields. In the first-harmonic time-resolved experiments, the altered population of the emitting exciton state was confirmed (Figure 6), but the change induced by the quadratic electric field effects was negligibly small, as discussed above. This difference between the first-order and quadratic field effects in the relaxation path k_2 of the hot exciton is ascribed to the dependence of k_2 on the direction of the externally applied electric field. In contrast with k_2, k_4 in Figure 8 seems to show both linear and quadratic field effects.

As the origin of the dependence on the field direction of the PL intensity and lifetime, the presence of an internal electric field is considered in a P3HT solid film sandwiched between FTO and PMMA as reported in multilayer films.[13,25−29] The scheme of energy levels of the device used in the present work is shown in Figure 9.[30−32] In general, an inherent potential exists at the interface between distinct materials, because of the difference of the Fermi levels; P3HT and PMMA serve as p-type semiconductor and hole-blocking layer, respectively. The internal field ($\boldsymbol{F}_{int}$) that has a negative direction shown in Figure 1 is considered to locate in P3HT, besides the external electric field ($\boldsymbol{F}_{ext}$). In the results, the total field given by the sum of $\boldsymbol{F}_{int}$ and $\boldsymbol{F}_{ext}$ increases, when $\boldsymbol{F}_{ext}$ is applied in the same direction as the internal field. When the external electric field is applied in the opposite direction, i.e., in the positive field direction, in contrast, the magnitude of the total field decreases. Even when $\boldsymbol{F}_{ext}$ is zero, $\boldsymbol{F}_{int}$ affects the P3HT photodynamic processes. With increased total electric field, i.e., with a negative field direction, both $k_1/(k_1 + k_2 + k_3)$ and $1/(k_4 + k_5 + k_6)$ in Figure 8 decrease, assuming that carrier generation is more promoted with an external electric field; that is, k_2 and k_4 increase with increasing total electric field. In

DOI: 10.1021/acs.jpcc.9b02946
J. Phys. Chem. C 2019, 123, 12647−12658

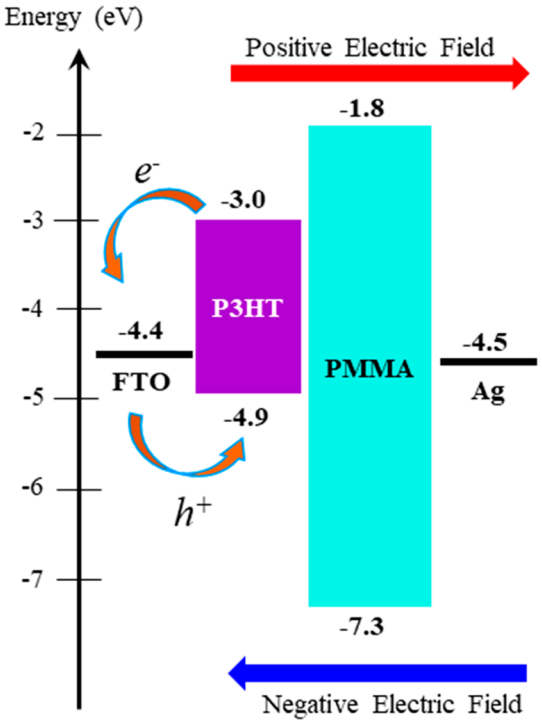

Figure 9. Energy levels of materials in the present work. The curved arrows indicate the direction of the diffusion of each photogenerated carrier. The straight red and blue arrows define the direction of the external electric field used in this work.

the results, both the population of the emitting state of the exciton and the lifetime of the exciton emission decrease on application of an external electric field in the negative direction. When an external electric field is applied in the positive direction, in contrast, the total electric field decreases, resulting in both increased population of the emitting state of the exciton and an increased lifetime of exciton emission, as observed. We hence conclude that both the internal electric field $\boldsymbol{F}_{int}$ that points in a negative direction and $\boldsymbol{F}_{ext}$ synergistically affect the dynamics of the G1 and G2 emitting states. The individual crystalline aggregates can spatially orient the transition dipole moments. This anisotropy of the dipoles leads to an observed dependence of the field direction, if the anisotropy were present, but the dipole orientation of the aggregates is expected to be random and isotropic, as an ensemble average. The anisotropy that originates from the orientation of the dipole of the aggregates is hence expected to be negligible.

When the effect of an electric field on the PL of a P3HT film sandwiched between FTO and PMMA films is compared with that of a P3HT film sandwiched between TiO_2 and PMMA films or a P3HT film sandwiched between Sb_2S_3 and PMMA films, the quadratic field effect is similar; PL is enhanced by $\boldsymbol{F}_{ext}$, and the lifetime increases in the presence of $\boldsymbol{F}_{ext}$ in a similar manner for both G1 and G2 bands, which results from a field-induced deceleration of the nonradiative decay in the PL emitting state. The PL of P3HT polymers doped in a PMMA film shows a similar quadratic field effect.[18]

Regarding the linear electric field, we mention some difference of the P3TH film sandwiched between FTO and PMMA films from the P3HT film sandwiched between TiO_2 or Sb_2S_3 and PMMA films. The linear electric field effect on the PL is negligible for P3HT polymers doped in a PMMA film.[31] As already reported,[8] the PL intensity of the G1 and G2 bands increased and decreased in a P3HT film sandwiched between TiO_2 or Sb_2S_3 and PMMA films in the presence of an external electric field with positive and negative directions, respectively, as a linear field effect, which is similar to the present result. We showed that the field-induced change of the intensity of the G1 band of maximum intensity at 705 nm results from only the field-induced change in the PL lifetime, but the population of the emitting state of G1 was unaffected on application of an electric field. In the G2 band, in contrast, not only the rate of nonradiative decay but also the population of the emitting state were affected by $\boldsymbol{F}$. In the present results, the linear field effect of G2 is similar to that for P3HT sandwiched between TiO_2 or Sb_2S_3 and PMMA films; both the population and lifetime of the emitting state of G2 are affected by $\boldsymbol{F}_{ext}$. The G1 band of the present sample showed a linear field effect similar to that of the G2 band; both the population and the lifetime of the emitting state of G1 were affected by $\boldsymbol{F}_{ext}$. The linear field effect of the G1 band of a P3HT film sandwiched between FTO and PMMA films differs from that of P3HT sandwiched between TiO_2 or Sb_2S_3 and PMMA films (cf. Figures 6c,d of the present results and Figures 10g,h and 11g,h of ref 8). These results indicate that the emitting state of G1 exists near the interface between FTO and P3HT; the nonradiative process of hot excitons that competes with relaxation to the emitting state of G1 is efficiently affected on application of an electric field, in contrast with a P3HT film in contact with TiO_2 or Sb_2S_3 film. In the hot excitons that relax to the G1 emitting state, the rate of carrier generation, i.e., k_2 in Figure 8, is considered to be much larger for hot excitons located on or near the FTO film surface than for hot excitons located on or near TiO_2 or the Sb_2S_3 film surface.

We simulated the observed decay curve of PL on assuming a triple exponential-decay function. Measurements of time-resolved fluorescence and transient absorption for P3HT films reported by other groups also showed complicated decay kinetics that could not be simulated with a single exponential decay.[18,20,33−35] The suggested origins of the complicated kinetics include the delayed PL because of charge recombination, exciton migration, and a structural relaxation of the P3HT chains.

5. CONCLUSION

E-A and E-PL spectra, that is, the field-induced change in absorption and PL spectra and the field-induced change in PL decay profiles, have been recorded for P3HT solid films sandwiched between a conducting layer of FTO and an insulator film of PMMA. On the basis of the E-A spectra, the magnitudes of the variation of the electric dipole moment and in polarizability following absorption were determined for P3HT sandwiched between FTO and PMMA; the results are compared with those for P3HT films in multilayer FTO/TiO_2/P3HT/PMMA/Ag and FTO/TiO_2/Sb_2S_3/P3HT/PMMA/Ag. The photoexcited state of P3HT sandwiched between FTO and PMMA films is shown to have charge-transfer character less than that of P3HT sandwiched between TiO_2 or Sb_2S_3 and PMMA films.

E-PL spectra of P3HT film sandwiched between FTO and PMMA films were recorded at both the first and second harmonics of the modulation frequency of $\boldsymbol{F}_{ext}$. A field-induced increase of both PL intensity and PL lifetime indicates that the rate of nonradiative decay at the PL emitting state is decelerated on application of $\boldsymbol{F}_{ext}$, as a quadratic field effect.

DOI: 10.1021/acs.jpcc.9b02946
J. Phys. Chem. C 2019, 123, 12647−12658

As a linear electric-field effect, the PL intensity is enhanced with F_{ext} for both G1 and G2, with a positive field direction, for which the positive electrode was connected to FTO and the negative electrode to silver. When the direction of F_{ext} was reversed, field-induced quenching of PL was observed for both bands. These results indicate that an internal electric field (F_{int}), which points in a negative direction, exists in the P3HT layer sandwiched between FTO and PMMA, as in the case of P3HT films sandwiched between TiO_2 or Sb_2S_3 and PMMA films.

The dependence of the PL intensity and lifetime on the direction of an applied field is attributed to the synergistic effect of F_{ext} and F_{int}. Depending on the direction of F_{ext}, the strength of the total electric field (F_{total}) that is given by the sum of F_{ext} and F_{int} also varies. The present results indicate that the strength of F_{total} increased or decreased, respectively, when F_{ext} was applied in negative or positive directions. Applied electric fields also induced an increased PL lifetime as a result of a quadratic field effect, resulting from a field-induced decreased rate of nonradiative decay at the PL emitting state. The field-induced increased or decreased population of the PL emitting state and the field-induced enhancement and quenching of the PL observed as the linear effect of an electric field are ascribed to the enhanced dissociation of both hot excitons and relaxed excitons in the presence of an electric field.

On the basis of our analysis of the quadratic and linear field effects on the PL decay profiles, the field-induced changes of both lifetime and preexponential factor were determined for each effect. A field-induced enhancement of PL intensity as a linear field effect observed with a positive field direction is attributed to both an increased population of the emitting states for G1 and G2 and a decreased rate of nonradiative decay of these emitting states. A field-induced quenching of PL of P3HT observed as a linear field effect with a negative field direction was attributed to a field-induced decrease of the population of the emitting states of G1 and G2 and to the field-induced enhancement of the rate of nonradiative decay of these states. The linear field effect of P3HT sandwiched between FTO and PMMA films on PL thus shows a field-induced variation of the population of the emitting state on PL for both G2 and G1 bands, in contrast with a P3HT film sandwiched between TiO_2 or Sb_2S_3 and PMMA films, for which the population of the emitting state of G1 is independent of the applied electric field in both quadratic and linear effects.

AUTHOR INFORMATION

Corresponding Authors

*(E.W.-G.D.) E-mail: diau@mail.nctu.edu.tw.

*(N.O.) E-mail: nohta@nctu.edu.tw.

ORCID

Kamlesh Awasthi: 0000-0001-7852-059X

Toshifumi Iimori: 0000-0003-2158-4378

Eric Wei-Guang Diau: 0000-0001-6113-5679

Nobuhiro Ohta: 0000-0003-4255-6448

Notes

The authors declare no competing financial interest.

ACKNOWLEDGMENTS

Taiwan Ministry of Science and Technology (MOST) provided financial support of this research (MOST 107-2113-M-009-005, MOST 108-3017-F-009-004, and MOST 105-2119-M-009-011-MY3). This work was financially supported also by the Center for Emergent Functional Matter Science of National Chiao Tung University from The Featured Areas Research Center Program within the framework of the Higher Education Sprout Project by the Ministry of Education (MOE) in Taiwan.

REFERENCES

(1) Yu, G.; Gao, J.; Hummelen, J. C.; Wudl, F.; Heeger, A. J. Polymer Photovoltaic Cells: Enhanced Efficiencies via a Network of Internal Donor-Acceptor Heterojunctions. *Science* **1995**, *270*, 1789−1791.

(2) Günes, S.; Neugebauer, H.; Sariciftci, N. S. Conjugated Polymer-Based Organic Solar Cells. *Chem. Rev.* **2007**, *107*, 1324−1338.

(3) Cheng, Y. J.; Yang, S. H.; Hsu, C. S. Synthesis of Conjugated Polymers for Organic Solar Cell Applications. *Chem. Rev.* **2009**, *109*, 5868−5923.

(4) Kang, H.; Lee, W.; Oh, J.; Kim, T.; Lee, C.; Kim, B. J. From Fullerene−Polymer to All-Polymer Solar Cells: The Importance of Molecular Packing, Orientation, and Morphology Control. *Acc. Chem. Res.* **2016**, *49*, 2424−2434.

(5) Kaloni, T. P.; Giesbrecht, P. K.; Schreckenbach, G.; Freund, M. S. Polythiophene: From Fundamental Perspectives to Applications. *Chem. Mater.* **2017**, *29*, 10248−10283.

(6) Cook, S.; Furube, A.; Katoh, R. Analysis of the Excited States of Regioregular Polythiophene P3HT. *Energy Environ. Sci.* **2008**, *1*, 294−299.

(7) Mehata, M. S.; Hsu, C. S.; Lee, Y. P.; Ohta, N. Electric-Field-Induced Enhancement/Quenching of Photoluminescence of π-Conjugated Polymer S3-PPV: Excitation Energy Dependence. *J. Phys. Chem. B* **2010**, *114*, 6258−6265.

(8) Iimori, T.; Awasthi, K.; Chiou, C. S.; Diau, E. W. G.; Ohta, N. Influence of External Electric Fields on Photoluminescence and Charge Carrier Dynamics of π-Conjugated Polymer P3HT in Multilayer Films with Heterojunctions to TiO_2 and Sb_2S_3. *ACS Appl. Energy Mater.* **2018**, *1*, 6136−6151.

(9) Boxer, S. G. Stark Realities. *J. Phys. Chem. B* **2009**, *113*, 2972−2983.

(10) Ohta, N. Electric Field Effects on Photochemical Dynamics in Solid Films. *Bull. Chem. Soc. Jpn.* **2002**, *75*, 1637−1655.

(11) Awasthi, K.; Du, K. B.; Wang, C. Y.; Tsai, C. L.; Hamada, M.; Narra, S.; Diau, E. W. G.; Ohta, N. Electroabsorption Studies of Multi-Colored Lead Halide Perovskite Nanocrystalline Solid Films. *ACS Photonics* **2018**, *5*, 2408−2417.

(12) Umeuchi, S.; Nishimura, Y.; Yamazaki, I.; Murakami, H.; Yamashita, M.; Ohta, N. Electric Field Effects on Absorption and Fluorescence Spectra of Pyrene Doped in a PMMA Polymer Film. *Thin Solid Films* **1997**, *311*, 239−245.

(13) Awasthi, K.; Wang, C. Y.; Fathi, A.; Narra, S.; Diau, E. W. G.; Ohta, N. Anisotropic Electric Field Effect on the Photoluminescence of $CH_3NH_3PbI_3$ Perovskite Sandwiched Between Conducting and Insulating Films. *J. Phys. Chem. C* **2017**, *121*, 22700−22706.

(14) Tsushima, M.; Ushizaka, T.; Ohta, N. Time-Resolved Measurement System of Electrofluorescence Spectra. *Rev. Sci. Instrum.* **2004**, *75*, 479−485.

(15) Liptay, W. Dipole Moments and Polarizabilities of Molecules in Excited Electronic States. *Excited States* **1974**, *1*, 129−229.

(16) Locknar, S. A.; Chowdhury, A.; Peteanu, L. A. Matrix and Temperature Effects on the Electronic Properties of Conjugated Molecules: An Electroabsorption Study of *all-trans* Retinal. *J. Phys. Chem. B* **2000**, *104*, 5816−5824.

(17) Jalviste, E.; Ohta, N. Theoretical Foundation of Electroabsorption Spectroscopy: Self-Contained Derivation of the Basic Equations with the Direction Cosine Method and the Euler Angle Method. *J. Photochem. Photobiol., C* **2007**, *8*, 30−46.

(18) Iimori, T.; Awasthi, K.; Chiou, C. S.; Diau, E. W. G.; Ohta, N. Fluorescence Enhancement Induced by Quadratic Electric-Field

DOI: 10.1021/acs.jpcc.9b02946
J. Phys. Chem. C 2019, 123, 12647−12658

Effects on Singlet Exciton Dynamics in Poly(3-hexylthiophene) Dispersed in Poly(methyl methacrylate). *Phys. Chem. Chem. Phys.* **2019**, *21*, 5695−5704.
(19) Clark, J.; Silva, C.; Friend, R. H.; Spano, F. C. Role of Intermolecular Coupling in the Photophysics of Disordered Organic Semiconductors: Aggregate Emission in Regioregular Polythiophene. *Phys. Rev. Lett.* **2007**, *98*, 206406.
(20) Guo, J.; Ohkita, H.; Benten, H.; Ito, S. Near-IR Femtosecond Transient Absorption Spectroscopy of Ultrafast Polaron and Triplet Excitation Formation in Polythiophene Films with Different Regioregularities. *J. Am. Chem. Soc.* **2009**, *131*, 16869−16880.
(21) Kawabata, H.; Ohta, N.; Arakawa, H.; Ashida, M.; Kohtani, S.; Nakagaki, R. Evidence for Electric-Field-Assisted Back-Electron Transfer Through a Methylene Bond in a Linked Compound of Phenanthrene and Phthalimide in a Polymer Film. *J. Chem. Phys.* **2001**, *114*, 7723−7726.
(22) Awasthi, K.; Ohta, N. Magnetic Field Effects on Electro-Photoluminescence of Photoinduced Electron Transfer Systems in a Polymer Film. *J. Photochem. Photobiol., A* **2011**, *221*, 1−12.
(23) Liess, M.; Vardeny, Z. V.; Lane, P. A. Electromodulation of Charge-Transfer Photoexcitations in Pristine and C_{60}-Doped Conjugated Polymers. *Phys. Rev. B: Condens. Matter Mater. Phys.* **1999**, *59*, 11053−11061.
(24) Kersting, R.; Lemmer, U.; Deussen, M.; Bakker, H. J.; Mahrt, R. F.; Kurz, H.; Arkhipov, V. I.; Bässler, H.; Göbel, E. O. Ultrafast Field-Induced Dissociation of Excitons in Conjugated Polymers. *Phys. Rev. Lett.* **1994**, *73*, 1440−1443.
(25) Kron, G.; Rau, U.; Werner, J. H. Influence of the Built-in Voltage on the Fill Factor of Dye-Sensitized Solar Cells. *J. Phys. Chem. B* **2003**, *107*, 13258−13261.
(26) Dong, C.; Li, X.; Zhao, W.; Jin, P.; Qi, J. Theoretical Analysis of Built-in Interfacial Electric Dipole Field in Dye-Sensitized Solar Cells. *J. Phys. Chem. C* **2013**, *117*, 9092−9103.
(27) Kniepert, J.; Schubert, M.; Blakesley, J. C.; Neher, D. Photogeneration and Recombination in P3HT/PCBM Solar Cells Probed by Time-Delayed Collection Field Experiments. *J. Phys. Chem. Lett.* **2011**, *2*, 700−705.
(28) Mingebach, M.; Deibel, C.; Dyakonov, V. Built-in Potential and Validity of the Mott-Schottky Analysis in Organic Bulk Heterojunction Solar Cells. *Phys. Rev. B: Condens. Matter Mater. Phys.* **2011**, *84*, 153201.
(29) Kemerink, M.; Kramer, J. M.; Gommans, H. H. P.; Janssen, R. A. J. Temperature-Dependent Built-in Potential in Organic Semiconductor Devices. *Appl. Phys. Lett.* **2006**, *88*, 192108.
(30) Lindblad, R.; Cappel, U. B.; O'Mahony, F. T.; Siegbahn, H.; Johansson, E. M.; Haque, S. A.; Rensmo, H. Energy Level Alignment in TiO_2/Metal Sulfide/Polymer Interfaces for Solar Cell Applications. *Phys. Chem. Chem. Phys.* **2014**, *16*, 17099−17107.
(31) Takanezawa, K.; Tajima, K.; Hashimoto, K. Efficiency Enhancement of Polymer Photovoltaic Devices Hybridized with ZnO Nanorod Arrays by the Introduction of a Vanadium Oxide Buffer Layer. *Appl. Phys. Lett.* **2008**, *93*, No. 063308.
(32) Wu, C.; Li, F.; Guo, T. Efficient Tristable Resistive Memory Based on Single Layer Graphene/Insulating Polymer Multi-Stacking Layer. *Appl. Phys. Lett.* **2014**, *104*, 183105.
(33) Banerji, N.; Cowan, S.; Vauthey, E.; Heeger, A. J. Ultrafast Relaxation of the Poly(3-hexylthiophene) Emission Spectrum. *J. Phys. Chem. C* **2011**, *115*, 9726−9739.
(34) Ferreira, B.; da Silva, P. F.; Seixas de Melo, J. S.; Pina, J.; Maçanita, A. Excited-State Dynamics and Self-Organization of Poly(3-hexylthiophene) (P3HT) in Solution and Thin Films. *J. Phys. Chem. B* **2012**, *116*, 2347−2355.
(35) Paquin, F.; Latini, G.; Sakowicz, M.; Karsenti, P.-L.; Wang, L.; Beljonne, D.; Stingelin, N.; Silva, C. Charge Separation in Semicrystalline Polymeric Semiconductors by Photoexcitation: Is the Mechanism Intrinsic or Extrinsic? *Phys. Rev. Lett.* **2011**, *106*, 197401.

DOI: 10.1021/acs.jpcc.9b02946
J. Phys. Chem. C 2019, 123, 12647−12658